Processes governing the recovery of a perturbed thermohaline circulation in HadCM3

Hadley Centre technical note 33

Michael Vellinga, Richard A. Wood, Jonathan M. Gregory

10 September 2001

Met Office

Abstract

In an experiment with the latest version of the Hadley Centre climate model we have analysed the model response after the thermohaline circulation ('THC') in the Atlantic Ocean has been suppressed. The suppression is induced by a strong initial perturbation to the salinity distribution in the upper layer of the northern North Atlantic. The model is then allowed to adjust freely. Salinity gradually increases and deep water formation in the Greenland and Norwegian Seas restarts, later also in the Labrador Sea. The meridional overturning recovers after about 120 years. In the first few decades when the overturning is very weak surface air temperature is dominated by cooling of much of the Northern Hemisphere and weak warming of the Southern Hemisphere, leading to maximum global cooling of 0.9^oC. The disruption to the atmosphere's radiation balance results in a downward flux anomaly at the top of the atmosphere, maximally $0.55 Wm^{-2}$ in the first decade then decreasing with the THC recovery.

We examine in detail the processes responsible for the recovery of the THC. This will help us in future model development to reduce uncertainty in modelling THC stability. The recovery is driven by coupled ocean-atmosphere response. Northward salt transport by the subtropical gyre is crucial to the recovery of salinity in the North Atlantic. A southward shift of the ITCZ creates positive salinity anomalies in the tropical North Atlantic. This supports the northward salt transport by the subtropical gyre that helps to restart deep water formation and the THC.

Processes governing the recovery of a perturbed thermohaline circulation in HadCM3

Michael Vellinga, Richard A. Wood, Jonathan M. Gregory

September 10, 2001

1 Introduction

One of the open questions in climate research is what determines the stability of the modern thermohaline circulation of the ocean ('THC'). The importance of this question to understanding climate behaviour lies in the strong influence on climate of the THC. In the present era significant changes to climate would follow a collapse of the THC (Manabe and Stouffer (1997)). Analysis of paleoclimate records seem to confirm the notion that the strong fluctuations of the last glacial period (Heinrich events and Dansgaard-Oescher cycles) were not only accompanied by cooling and freshening of the surface of the north Atlantic (Cortijo *et al* (2000)), but in certain cases by reduced volumes of North Atlantic Deep Water (Keigwin *et al* (1991); Muscheler *et al* (2000)). To what extent the role of the THC in these climatic excursions was active rather than passive is still unclear from paleorecords (Boyle (2000)). That the THC at least has the potential of being actively involved in these rapid climate transitions has been demonstrated in numerical experiments by Ganapolski and Rahmstorf (2001).

Unfortunately, there is uncertainty as to the degree of stability of the modern THC. The weakening of the THC over the next century, as predicted by various climate general circulation models (GCMs), in response to an increase in greenhouse gas concentrations ranges from 0-50% (Cubasch *et al* (2001)). We know from experiments described by Manabe and Stouffer (1988); Manabe and Stouffer (1999a) that with present-day insolation the GFDL climate model has two possible climate states: one with and one without North Atlantic Deep Water ('NADW') formation, and associated presence or absence of N-Atlantic THC. This behaviour of the THC in the GFDL model seems consistent with findings by Rahmstorf (1996) that due to hysteresis behaviour of its THC an ocean GCM can have equilibrium states with and without NADW formation for a given set of model parameters. Whether or not other climate models have a similar multiplicity of equilibria is unclear. In a freshwater perturbation experiment with the ECHAM3/LSG model Schiller *et al* (1997) did not find a stable state without NADW formation. To succesfully trigger a transition between equilibria may, however, require very large perturbations. Manabe and Stouffer (1995); Manabe and Stouffer (1997) perturbed the control state of the GFDL model, but this did not lead to the model state without a vigorous THC. Dijkstra and Neelin (2000) show that, for a zonally averaged ocean model, the extent of the hysteresis curve in parameter space shrinks with increasing latitudinal asymmetry of the surface freshwater flux, a feature that may differ between models.

To increase confidence in the predicted behaviour of the THC by GCMs it is important to identify the physical processes that control THC stability, understand how these work and, where necessary, improve on their representation in the model. The purpose of this study is to address the first two questions. We use HadCM3, the most recent version of Hadley Centre atmosphere-ocean general circulation model. We will describe how the model responds when the THC has been suppressed through a prescribed initial freshening of the northern North Atlantic. We will identify the physical processes that dominate the response in the model and therefore are key in determining the stability of the THC to this type of perturbation. This knowledge will assist our model development in the future to improve simulation of the stability of the THC.

To obtain a response that is solely due to the disruption of the THC the experiment is carried out with fixed, pre-industrial greenhouse gas conditions. Other studies analyse the THC in HadCM3 under increased greenhouse gas concentration (Wood *et al* (1999); Thorpe *et al* (2001)) and last glacial maximum conditions (Hewitt *et al* (2001)).

An important difference between experiments described in the literature (e.g. Manabe and Stouffer (1997),Schiller *et al* (1997)) and the one described here is that the HadCM3 model does not use flux adjustment. Flux adjustment modifies the relation between heat transport and model state and may thus deform the model's dynamical properties (Dijkstra and Neelin (1999)). So it is valuable to understand the THC response in absence of flux adjustment. Furthermore, the grid resolution of HadCM3, while still coarse, does allow us to distinguish between deep water formation in the Labrador, Greenland and Norwegian Seas. Wood *et al* (1999) have demonstrated the potential for differing behaviour of deep water formation in these regions when the model is forced by increased greenhouse gas concentrations.

A description of the model and the set-up of the experiment is given in section 2. We discuss in section 3 those aspects of the climate response that are relevant to global climate and the THC recovery. Other aspects of the climate response that are not essential to understand the THC recovery, but which may be relevant to climate impact studies are presented in a separate paper (Vellinga and Wood (2001)). The recovery of the THC itself is discussed in section 4. Discussion and conclusions follow in section 5.

2 Model properties and set-up of experiment

The climate model that has been used in this study is HadCM3, a coupled ocean-atmosphere model, with sea-ice and land surface schemes. The atmosphere model has a resolution of $2.5^o \times 3.75^o$, with 19 vertical levels. The ocean model is based on that of Cox (1984) and has a resolution of $1.25^o \times 1.25^o$ with 20 vertical levels, 10 of which are in the top 300m. The model maintains a stable surface climate throughout a control run with fixed pre-industrial greenhouse gas concentrations for over 1000 years without the use of flux correction. Details of the model and an assessment of its control climate are given by Gordon *et al* (2000) and Pope *et al* (2000). That experiment will be referred to as 'control run' in this paper. Aspects of the ocean component of the coupled model have been discussed before: global ocean heat transport by Gordon *et al* (2000); the Indonesian throughflow and circulation in the Indian Ocean by Banks (2000a); circulation and heat transport in the South Atlantic by Banks (2000b).

Before we describe the set-up of the perturbation experiment it is worthwhile to show the THC in HadCM3 during the control run. A common perception of the thermohaline

circulation is that of a global circuit: the southward flow of NADW and compensating northward return flow of warm water in the North Atlantic require a transformation of water masses on a global scale (e.g. Broecker (1991)). If the the horizontal flow is partitioned in cold and warm water masses (Fig. 1a,b) the major pathways of the THC appear: the overflow from Denmark Strait; the deep western boundary current that flows into the Southern Ocean where it meets a strong Antarctic Circumpolar Current (ACC); northward flow of cold water into the South Pacific Ocean. In the Indian Ocean the cold flow is dominated by the Indonesian Throughflow and flow in the Mozambique Channel; there is only weak flow into the Indian Ocean across 32^oS. More about the circulation in the Indian Ocean can be found in Banks (2000a). In the warm water limb the major western boundary current systems emerge, as well as the extension of the Indonesian throughflow and the confluence in the South Atlantic towards South America. Sites where heating of the upper $1000\,m$ of the ocean due to convection is strong are in the Nordic Seas and off the Antarctic shelf (shading, Fig. 1a).

Various estimates of integrated mass transports based on inversions of hydrographic sections exist (Macdonald (1998); de las Heras and Schlitzer (1999); Ganachaud and Wunsch (2000)), and can be used to validate HadCM3 transports. Here we follow Macdonald (1998) who uses a two way classification of the transport into warm and cold water masses. Temperatures in the Atlantic Ocean predicted by HadCM3 are too warm (Gordon *et al* (2000)) so we adapt the 5.5^oC isotherm as the boundary between 'cold' and 'warm' water masses instead of the 3.5^oC isotherm used by Macdonald (1998). Beyond the Atlantic and Southern Ocean the model transports do not differ by more than about $2\,Sv$ between either definition of the temperature boundary. Model transports and observational estimates across several ocean cross sections may be compared in Table 1. The major discrepancies between HadCM3 and the inverse model are: the flow across 48^oN in the Atlantic, which is too weak; the weak cold inflow into the Indian Ocean across 32^oS; and too strong transports by the ACC. Apart from these discrepancies and the fact that the 'base' temperature in the Atlantic is too warm, HadCM3 models the global circulation reasonably well.

We have produced a weakened THC in the model by perturbing the state that the control integration had reached after 100 years. We modified this original state by replacing the salinity field in the top 800m of the North Atlantic ($[80^oW-20^oE]\times[50^oN-90^oN]$) with a vertical profile that is much fresher, and has a deeper pycnocline (Fig. 2). On average, the water in the area of the perturbation is made 2 psu fresher. Assuming a reference salinity of 35 psu, the area would have to receive a freshwater pulse of about $6\cdot10^{14}m^3(\approx 16\,Sv*year; 1\,Sv\equiv10^6m^3s^{-1})$ to experience this freshening. Conservation of salt was assured by globally redistributing the salt taken out of the North Atlantic, increasing salinity everywhere by about 0.01 psu. The model was allowed to adjust freely to the new salinity field in an integration of 150 years. Various aspects of the adjustment process are discussed in the following sections.

3 Climate response

In this section we analyse major changes in climate in response to the freshwater perturbation. Response in the Atlantic ocean is described in sec. 3a: circulation , ocean heat transport and deep water formation. Response in the atmosphere is described in section 3b. We will focus on air temperature and aspects of the radiation budget, as well

as the response in the tropics. The recovery of the THC is discussed in section 4. The focus here is mainly on climate response that is relevant to the recovery of the THC. Other climate impacts from the disruption of the THC are described by Vellinga and Wood (2001).

Anomalies are calculated with respect to the parallel part of the control integration. They are deemed significant if exceeding two standard deviations calculated from the parallel period of the control run.

a The ocean

The initial freshening applied to the North Atlantic creates an instantaneous change to density, to which the circulation has to adjust. It has been shown elsewhere that adjustment of the ocean to a given density field occurs through Kelvin and Rossby wave propagation, on timescales from several months to decades (e.g. Kawase (1987); Johnson and Marshall (2001)). This stage of the adjustment is not described here. In the control run the zonal mean circulation in the Atlantic is dominated by northward flow in the top 600 meters and southward flow of NADW between 600-4000m (Fig 3a). In the Southern Hemisphere is a deep cell with opposite sense of circulation. In the first ten years after the freshwater was put in the northern Atlantic, the basinwide NADW overturning cell has disappeared (Fig 3b). The maximum overturning has weakened to $8\,Sv$ in the Southern Hemisphere, and $4\,Sv$ in the Northern Hemisphere. The circulation has become more shallow. In the North Atlantic is a negative cell with weak *upwelling* around 50^oN. In years 20-30, this negative cell has disappeared, with weak sinking of $4\,Sv$ around 60^oN (Fig 3c). There is about $8\,Sv$ of shallow overturning in the subtropics but the connection between the South and North Atlantic has been lost, with detached overturning cells near 30^oN and 30^oS. The deep cell slowly expands further to the north and intensifies. The NADW cell recovers at a rate of about 1.3 Sv/decade and it takes about 120 years before the THC has regained its original strength (Fig 3d). The condition that we forced HadCM3 into, with a fresh North Atlantic and weak northern sinking, is not a stable state.

The weakening of the meridional overturning causes a significant reduction in the northward heat transport in the Atlantic Ocean, up to $0.6\,PW$ in years 20-30 (Fig. 4a). The reduction in the transport by the overturning is latitude dependent: it increases from $-0.3\,PW$ at 30^oS (reduced interbasin exchange) to $-0.8\,PW$ at 20^oN (lack of vigorous overturning *within* the Atlantic). There is some compensating northward heat transport by the North Atlantic subtropical gyre, but the northward transport by the subpolar gyre weakens. The corresponding changes in the meridional freshwater transport are shown in Fig. 4b. Changes at 30^oS (weaker northward transport) and in the North Atlantic (stronger southward transport) are small but essential to remove the perturbation. Strong compensation between changes in the transport by the meridional overturning and the gyre maintain southward freshwater transport in the northern (sub)tropical Atlantic. This is discussed in detail in Sec. 4.

The core areas where the model forms its NADW have different responses to the freshwater perturbation (Fig.5). Downwelling in the Greenland and Norwegian Seas, in the first decade completely suppressed by the freshening of the top layer, starts again from the second decade. It takes only 50 years to recover fully, and overshoots the original production rate. It will be shown in section 4 that in the first decade of the experiment the Norwegian and Greenland Sea cool and that part of the fresh anomaly

is transported out of the region. These two effects lead to conditions under which deep water formation can recover.

Downwelling associated with mixing over and downstream of the overflow sills restarts by year 50, when the overflow has become dense enough again. By contrast, deep water formation in the Labrador Sea does not resume during the first 100 years after the perturbation. Extensive wintertime sea ice cover in the Labrador Sea (Fig. 6) isolates the surface ocean from the overlying air, and prevents the surface heat loss necessary for strong convection. Changes to the nature of sea ice formation in the Labrador Sea are hindering deep water formation. Under control climate conditions the Labrador Sea is an area where a net production is roughly balanced by export of sea ice, giving a net export of freshwater (Fig. 7a). Between years 10-40 of the perturbation run the situation is reversed: a net import of sea ice —mainly from the Greenland Sea and carried by the East Greenland Current— is balanced by melt, resulting in a net freshwater input at the surface. This is a positive feedback to the original perturbation. It is not until the sea ice cover has returned to normal that upper layers can grow dense enough for convection and deep water formation to occur. In the GIN Seas the situation is precisely the opposite (Fig. 7b). In the control climate (southward) ice transport from the Arctic is the dominant source of sea ice in the GIN Sea, and is balanced by local melt. This constitutes a surface freshwater input. In the first few decades of the perturbation experiment, local formation of sea ice is more important than in the control run. The increase in ice formed in the GIN Sea is roughly balanced by export of sea ice. Compared to the large import of sea ice during the control run this constitutes a freshwater export, acting to restore surface salinity, and is a negative feedback. The different response of deep water formation in the Labrador Sea and GIN Sea to external perturbations has been noted before (Wood *et al* (1999)).

Schiller *et al* (1997) describe how significantly increased wind-driven (Ekman) upwelling in the Nordic Seas (up to 16 standard deviations) drives a barotropic flow that transports freshwater away from the convection areas. It also compresses isopycnals near the surface, which destabilises the water column. In the ECHAM3/LSG model this upwelling feedback is very important in restarting the THC. HadCM3 is different in two respects. Firstly, anomalies in the vertical Ekman velocity, as calculated from the surface wind stress, are significant in parts of the Greenland and Norwegian Seas (up to four standard deviations) and south of Greenland (up to six standard deviations, Fig. 10a). This is far weaker than the response in the ECHAM3/LSG model. Secondly, anomalies in vertical velocity near the surface are weaker than those found by Schiller *et al* (1997), and are not as strongly dominated by the wind stress curl, notably near the overflows and coast lines. The numerous differences in model formulation between HadCM3 and ECHAM3/LSG (geostrophic vs. non-geostrophic, rigid-lid vs. free surface), horizontal and vertical grid resolution and topography could account for the difference in this aspect of the response.

We will show in Sec. 4 that freshwater transport by the North Atlantic gyre circulation plays an important role in the THC recovery. This section of the ocean response is therefore concluded by examining changes in the barotropic circulation in the North Atlantic. The two main features in the North Atlantic are the subtropical and subpolar gyres (Fig. 8a). Both gyres weaken in the perturbation experiment (Fig. 9). For the first ten years only we have full forcing fields of the barotropic flow available. Weakening of the subpolar gyre is fairly uniform, but in the subtropical gyre is concentrated near the recirculation off Florida and near the Grand Banks (Fig. 8b). Changes in wind

forcing do not cause this change. At 60^oN the wind-driven Sverdup flow weakens by $15\,Sv$ (Fig. 8c), little elsewhere. The weakening of barotropic flow is dominated by the weakening of the bottom pressure torque (Fig. 8d). Changes to the viscous torque (not shown) cancel the changes induced by the bottom pressure torque and wind stress in the area around Greenland. In the perturbation experiment the overflows and the Deep Western Boundary Current weaken, which changes the (vertical) bottom velocity. Vertical bottom velocity near topography creates a bottom pressure torque that forces the barotropic flow (Holland (1973)), and a similar mechanism mechanism exists in Bryan-Cox type ocean models (Bell (1999)). Links between the strength of the THC and the barotropic flow have been noted before by Döscher *et al* (1994).

b The atmosphere

The altered ocean heat transport triggers major changes in SST. These feed back onto the atmosphere through the surface heat flux. We will limit our discussion here to surface air temperature and to the circulation in so far as this affects precipitation and evaporation which are important in understanding the THC recovery. Vellinga and Wood (2001) discuss additional surface climate variables.

The reduction of surface heat release in the North Atlantic causes significant cooling of surface air temperature. Maximum cooling of 8^oC occurs over the northwest Atlantic, while over the bordering continental landmasses the air cools by $2-4^oC$ (Fig. 11). The region with the strongest sea surface temperature (SST) cooling is actually the *northeast* Atlantic (not shown). The increased sea-ice cover of the Labrador Sea and the Reykjanes Basin mentioned before generate the very low surface air temperatures over the *northwest* Atlantic (Fig. 6). Sea ice cover in the GIN Sea, on the other hand, is not fundamentally different from the control climate, save for the first decade, and the westward retreat of the sea ice margin in the Greenland Sea. Significant cooling up to 2^oC occurs over Asia. The cold air flows out over the North Pacific which results in stronger heat loss by the ocean. In the Southern Hemisphere the air over the Atlantic warms by $0-1^oC$, with further isolated areas where anomalous heating emerges from the natural variability. In the Southern Ocean warm SST anomalies from the South Atlantic propagate eastwards on the ACC. The temperature anomaly is comparable to the response reported by Manabe and Stouffer (1997) in their meltwater experiment with the GFDL model.

Global average surface air temperature is about 0.9^oC cooler in the first decade of the experiment than in the control run (Fig.12a). This is highly significant: the decadal mean standard deviation for the control run is about 0.06^oC. During the following 50 years air temperature gradually recovers, and towards the end of the experiment becomes slightly warmer than in the control run. During the 50 years of depressed global temperature there is a positive anomaly (relative to the control) in the net TOA flux (Fig. 12b, heavy solid line) that tends to warm climate as a whole. Given the relatively small heat capacity of the atmosphere and the land, most of the anomalous TOA flux is taken up by the ocean, which warms (volume-avarage temperature increases by 0.05^oC by year 50, not shown). Small imbalances between TOA and surface fluxes lead to the initial cooling and subsequent warming of the atmosphere. After year 50 temperature and TOA flux anomalies become small and are not discussed further. We can split the net downward radiation anomaly into components (all expressed as positive downwards, relative to control). These are: the anomalies in clear-sky longwave radiation ('LWR')

(i.e. the longwave radiation recalculated after the instantaneous removal of the clouds without any compensating adjustment), clear-sky shortwave radiation ('SWR'), and cloud radiative forcing (the difference between net downward radiation with and without clouds). The clear-sky LWR can be thought of as the basic radiative response of the atmosphere due to changes in temperature and amount of water vapour. The increase in this quantity is the response to the depressed temperatures. A linear fit of TOA clear-sky LWR flux and surface air temperature gives a sensitivity of $1.86 \pm 0.03\, Wm^{-2}K^{-1}$. Similar values were determined by Gregory and Mitchell (1997) for the previous version of the Hadley Centre climate model (HadCM2) when it was run under a two times CO_2 scenario with and without flux adjustment. We can thus identify the clear-sky LWR response as a process that operates with constant sensitivity under very different types of climate perturbations.

It is interesting to note that there is a close relation between the (anomalous) TOA clear-sky LWR flux and latent heat flux out of the ocean (Fig. 12b, dotted line). Like the surface air temperature, global average SST cools (Fig. 12a, dashed line), resulting in less evaporation and a smaller latent heat flux from the ocean. The associated latent heat release is no longer available to the atmosphere. The atmosphere heat budget adjusts to this by changing the outgoing clear-sky LWR.

The cooling of the ocean surface occurs mainly in years 0-3 (Fig. 12c, heavy solid). The global heat budget of the upper ocean shows that this cooling is mainly the result of changes in vertical mixing (Fig. 12c, dotted), which is consistent with the applied freshening. In response to the cooler SST the surface heat flux into the atmosphere adjusts (Fig. 12c, long dashes), and reduces the rate of cooling of SST from year 2 on. From year 4 onwards vertical mixing and surface flux are approximately in balance, and the temperature response is approximately set by (vertical) heat advection. Other terms in the heat budget are relatively weak. In the long term mixing is re-established and with the anomalous surface flux acts to restore SST (not shown).

The clear-sky SWR anomaly acts as radiative cooling (Fig. 12b, dash-dot) which implies a higher surface albedo than in the control run. Given the anomalously cold global air temperature in the first 50 years this is what one expects from the ice-albedo feedback. Anomalies of cloud radiative forcing (Fig. 12b, long dash) are small compared to the other fluxes.

In HadCM3, the disruption to the THC climate thus leads to a significant change in the TOA flux. To our knowledge there exists no relevant information in literature to compare this result to. But Manabe and Stouffer (1997); Manabe and Stouffer (1999b) report that no net global cooling occurred in their meltwater experiments. They found on average cancellation between Northern Hemisphere cooling and Southern Hemisphere warming, a result fundamentally different from ours.

In the extratropics the velocity response is generally geostrophic and tends to create anomalous south-westerly flow of moist subtropical air over the western North Atlantic (Fig. 13). Higher pressure over Europe reduces the penetration of maritime air and results in drier conditions. The strongest response in $E-P$ is found over the equatorial Atlantic. North of the equator $E-P$ increases by $4\, mm/day$, with a comparable decrease south of the equator. There is a cross equatorial southward moisture transport in the Atlantic, driven by anomalous southward low level winds.

The response in the tropics may be analysed in terms of the zonally averaged flow. For weak dissipation the dominant balance in the thermodynamic equation is between diabatic heating and vertical advection (Gill (1980); Pedlosky (1987)). In our experi-

ment we find that the most important term to change the amount of diabatic heating is latent heat release. For the vertically integrated, zonal mean heating the loss (gain) in the Northern (Southern) Hemisphere tropics amounts to $10\,Wm^{-2}$ (Fig. 14a). This anomalous cooling in the north and heating in the south forces an anomalous (annual mean) Hadley cell centred on the equator, with anomalous rising in the Southern Hemisphere, and anomalous sinking in the Northern Hemisphere, in effect shifting the ITCZ southwards. A similar response was described by Schiller *et al* (1997) in their meltwater experiment. The reduction in the annual mean atmospheric overturning scales well with the anomalous diabatic heating (Fig 14b, the anomalous heating is not perfectly symmetric around the equator). If one assumes a simple balance between the diabatic heating Q and vertical heat transport $w\partial\theta/\partial z$ the zonally averaged upwelling in a 15^o latitude band scales scales at about $2.2 \cdot Tg\,m^2 J^{-1}$ (neglecting covariance in non-zonality of the advection term and assuming that the anomalous diabatic heating is distributed uniformly over the depth of the troposphere, taken as 10 km; the average stratification is taken as $3\ K/km$). The sensitivity of the Hadley circulation in HadCM3 is, although stronger, of comparable magnitude to that predicted by the simple balance . Strong sensitivity of the Hadley circulation to details of the diabatic heating (e.g. the spatial structure) has been reported before (Hou and Lindzen (1992)).

The anomalous rising of the Hadley circulation in the Southern Hemisphere is consistent with the anomalous southward moisture transport across the equator (Fig. 13). The associated latent heat is now released in the Southern Hemisphere where it drives the anomalous rising. It is this change in latent heat release and not the change in boundary layer heating that causes the anomalous rising and sinking. In fact, the boundary layer heating changes to the extent that it warms the atmosphere north of the equator and cools it south of the equator, in spite of the sign of the SST anomaly. This may be caused by the change in wind stress, which weakens south of the equator and increases north of the equator.

The freshwater export across the equator is also the major anomaly in the surface freshwater balance of the equatorial North Atlantic (Fig. 15). It results in the initial doubling of the evaporation surplus to about $0.2Sv$. (in the control run $P-E \approx -0.2\,Sv$). We will see below that this evaporation stimulates the recovery of salinity in the North Atlantic Ocean.

Thorpe *et al* (2001) describe how in experiments where the model is forced with an IPCC IS92 scenario of increasing greenhouse gas concentrations there is an anomalous atmospheric freshwater flux out of the North Atlantic into the Pacific across Central America. This renders the surface waters in the tropical Atlantic more saline, and eventually acts to stabilise the THC. In our experiment we find this component of the hydrological cycle changes little. The reason may be that in our case the anti-symmetric SST pattern around the equator is the dominant feature and it drives the anomalous low-level winds. This pattern is absent in the greenhouse gas scenario run where other processes determine the atmospheric response, such as an enhanced hydrological cycle under warmer conditions.

4 Process of THC recovery

The process of recovery of the THC in the Atlantic Ocean is best understood by evaluating the evolution of density. A strong relation between the strength of the THC and the

meridional steric height gradient in the Atlantic was identified by Hughes and Weaver (1994) for equilibrium states in an ocean GCM and by Thorpe *et al* (2001) for a wide range of transient and equilibrium states in HadCM3. The current perturbation experiment has a similar relation between overturning and steric height gradient as Thorpe *et al* (2001) (not shown).

Contributions of potential temperature θ and salinity S to the rate of change of potential density σ can be estimated as:

$$\frac{\partial \sigma}{\partial t} = -\alpha \frac{\partial \theta}{\partial t} + \beta \frac{\partial S}{\partial t} + \cdots \tag{1}$$

where α and β are the respective linear coefficients of expansion. The non-linear terms in the equation of state are neglected in this analysis. Equation (1) is averaged in vertical and zonal directions (vertical and zonal averages will be indicated as $\langle\bar{\cdot}\rangle$). Model ouput enables us to distinguish between the physical processes that change temperature and salinity. The various processes are lumped together into two categories: changes due to surface fluxes and changes due to ocean transports:

$$\alpha \frac{\partial \langle\bar{\theta}\rangle}{\partial t} = -\alpha \frac{\partial}{\partial t} \left(\langle\bar{\theta}\rangle_{\text{surf}} + \langle\bar{\theta}\rangle_{\text{transp}} \right) \tag{2}$$

and similarly for $\langle\bar{S}\rangle$.

We have calculated decadal mean anomalies of all three terms in (2) with respect to their time averages from the control experiment (Fig.16). The *temperature response* is the result of a small imbalance between strong responses in the surface flux and heat transport (Fig. 16a). The strong reduction in the surface heat flux (cf. section 3a) appears here as anomalous warming to the North Atlantic (Fig. 16c). Conversely, the weakening of the THC means there is no longer an exchange of warm and cold water, and gives anomalous transport a cooling effect (Fig. 16e). In terms of density, the anomalous surface flux opposes the recovery of high-latitude density, while the total transport assists the recovery. The net temperature evolution is rather noisy and its effect on the evolution on density is weak compared to that of salinity.

Relevant to climate as the temperature evolution may be, it is the *salinity response* that in the end dominates the re-establishment of density in the North Atlantic (Fig. 16a,b). In the first decade anomalous transport by the negative overturning cell (section 3a, Fig. 3b) translates part of the initial freshwater perturbation southward from the area where it was introduced (i.e. southwards from $50^o N$, (Fig. 16b,f). North of this latitude relatively fresh water is replaced by water of normal salinity. After that first decade the response is generally one of salinity increase, and the original perturbation is eroded. North of about $20^o N$ anomalous freshening due to surface fluxes (Fig. 16d, cf. section 3b) is overcome by anomalous convergence of ocean salt transports (Fig. 16f). The southward shift of the ITCZ (sec. 3b) is apparent as a 'dipole' in the surface salinity flux around the equator (Fig. 16d). An anomalous divergence of salt transport shows that the equatorial North Atlantic is an area from which salt is extracted by ocean transports.

As another way to understand the recovery of salinity we show anomalies to the integrated freshwater budget of the Atlantic and of some subdomains (Fig. 17). The integrated surface freshwater input in the Atlantic is for most of the time not significantly changed by the disruption of the THC (Fig. 17a, dash-dot). $P-E$ and runoff anomalies

roughly compensate each other which suggests on average a shift of precipitation patterns but no net change in atmospheric moisture export from the Atlantic catchment area. Anomalous southward freshwater transport by the ocean across 30^oS (shown in Fig. 17b, dotted) creates a negative freshwater budget (Fig. 17a, solid). It shows that the response restores average salinity in the Atlantic: about $10\,Sv * year$ of freshwater has been shed after 150 years. The transport anomaly at 30^oS is caused by reduction in transport by the weakened meridional overturning (Figs. 3c,4b).

Changes of the freshwater budget within the Atlantic Ocean highlight the recovery of high-latitude salinity (Fig. 17b-d). In the South Atlantic (Fig. 17b) enhanced surface freshwater input is a result of the southward shift of the ITCZ discussed earlier (sec. 3b). In years 0-50 anomalous ocean transport across the equator exports about half the amount of freshwater brought in by surface flux anomaly back to the Northern Hemisphere. The remainder, about $0.1\,Sv$, actually leaves the basin as an anomalous freshwater transport across 30^oS. The net change in the fresh water budget of the South Atlantic is small up to year 80. By then the fresh water from the north starts to arrive.

A permanent, anomalous southward transport of fresh water across 25^oN carries the remnants of the initial perturbation away from the North Atlantic (Fig. 17c,d). Together with the anomalous northward transport across the equator this creates an anomalous convergence of freshwater transport between $0 - 25^oN$ for most of the experiment. The changes in the net freshwater budget between $0 - 25^oN$ are nevertheless small, apart from the first decade, due to the significant reduction of integrated $P - E$ associated with the shift of the ITCZ. After the first decade, freshwater from the North Atlantic (Fig. 17d) is routed southward, and not into the Arctic. Surface freshwater flux in the North Atlantic increases but this integrated $P - E$ anomaly is small compared to the anomalous ocean transport at 25^oN.

The freshwater transport at that latitude in the control run is dominated by southward transport through the meridional overturning. When in the perturbation run that transport is diminished because of the lack of overturning, freshwater transport by the subtropical gyre compensates by reversing sign (Fig. 18a), even though the strength of the subtropical gyre actually weakens by about 1/3 in the first few decades as shown previously (Fig. 9). This is due to anomalous positive correlation between v' and S' in the Atlantic, rather than negative correlation as in the control run: the eastern part of the basin is anomalously fresh due to the remnants from the initial perturbation, while in the west the ocean is anomalously saline. The gyre freshwater transport across 25^oN is crucial in the first five decades to replace fresh by saline water in the North Atlantic. When the meridional overturning has recovered sufficiently it takes over this role and carries most of the southward freshwater transport. The extra southward freshwater transport at 55^oN after year 10 is carried equally by all components (Fig. 18b).

From his conceptual model Rahmstorf (1996) concludes that the *equilibrium* state of the Atlantic THC is controlled by magnitude and direction of the 'active' freshwater flux across 30^oS (defined as the total freshwater flux into the catchment area of the Atlantic that is not carried by the THC itself) since this must be balanced by the freshwater transport of the THC. As emphasised by Rahmstorf (1996) transient behaviour such as in our experiment is not included in his analysis of the conceptual model. This is further illustrated by the fact that in the course of our experiment the anomalous 'active' freshwater import (essentially carried by a stronger South Atlantic gyre) is weaker than the anomalous export by the overturning (Fig. 17a, 'active' and 'MO30S'). In this section we have shown that processes within the Atlantic basin determine transient THC response.

5 Conclusions and discussion

To investigate which processes control the stability of the thermohaline circulation ('THC') in HadCM3 we have analysed the coupled response after the THC has been suppressed by instantaneous freshwater input in the North Atlantic. Within 10 years the THC weakens to about $4\,Sv$ in the Northern Hemisphere and shallows. This results in cooling of global air temperature of about 0.9^oC: cooling in the Northern Hemisphere dominates warming in the Southern Hemisphere. The THC gradually recovers over a period of about 120 years.

In our perturbation experiment we have not found a second stable climate state without a THC such as the one known to exist in the GFDL model (Manabe and Stouffer (1999a)). The existence of such a state in HadCM3 cannot be ruled out just on the basis of the current experiment, or on other relevant experiments carried out with HadCM3 (Wood *et al* (1999); Thorpe *et al* (2001); Hewitt *et al* (2001)). The disruption of the THC here results in a change of the atmospheric radiation balance. This gives a net downward TOA flux, violating an important condition for a stable, steady climate state.

The re-establishment of the THC in this experiment is closely linked to the recovery of density in the North Atlantic, that starts NADW formation. Evolution of density is largely determined by the evolution of salinity. We have identified three important processes that direct the recovery of the THC after its suppression. They are a mix of ocean and coupled ocean-atmosphere feedbacks. Firstly, the subtropical gyre transports salt from the subtropical North Atlantic northward to the midlatitudes, when the meridional overturning is no longer able to. This is the most important mechanism by which high-latitude salinity can recover. Dilution by anomalous surface freshwater flux in the midlatitudes is too weak to annul this gyre salt transport. Secondly, the southward shift of the ITCZ creates positive salinity anomalies north of the equator that compensate for the fresh water arriving from the North Atlantic. In the absence of the tropical salinity anomalies the efficiency of the northward salt transport by the gyre would be reduced and the rate of recovery of the THC would be slower. Finally, sea ice cover and deep water formation are closely related: anomalous winter time sea ice cover of the Labrador Sea prevents deep water formation there, the lack of persistent sea ice cover anomalies in the Greenland and Norwegian Seas allows deep water formation, that helps to start the THC again. To what degree all these processes depend on details of the perturbation (e.g its size or duration) is something we will investigate in the near future.

Having identified the processes that control the stability of the THC in HadCM3, the next step will be to validate them and to reduce the uncertainty in their representation. As the large scale global and Atlantic ocean freshwater budgets approach an equilibrium in the model control run, the overturning circulation transports freshwater into the Atlantic (Pardaens *et al* (2001)). This is in contrast to the net export of freshwater out of the Atlantic believed to be the case in the present day thermohaline circulation (Rahmstorf (1996); Weijer *et al* (1999)). That difference is due to an evaporative bias in the tropical and subtropical Atlantic of HadCM3 which leads to excessively saline NADW (Pardaens *et al* (2001)). This can have implications for stability of equilibrium states, since northward freshwater transport across 30^oS by the meridional overturning forms a stabilising feedback on the THC (sec. 4): a weakened THC means that less freshwater is transported into the Atlantic. Furthermore, any errors in the sensitivity of the tropical atmosphere to the Atlantic SST anomaly will introduce uncertainty about

the size of the tropical salinity anomaly. We believe, however, the response in the strength of the Hadley cell to the diabatic heating anomalies to be reasonable. We are currently examining the variability of the hydrological cycle of the tropical Atlantic and Pacific Oceans in the model, with the aim to compare the model sensitivity to re-analysis data (Schmittner *et al* (2000)).

The grid resolution of HadCM3 is fine enough to, say, distinguish between the marginal basins of the Nordic Seas and the different response in deep water formation regions. But grid spacing is still far too coarse to resolve many small-scale features and processes. Insufficient grid resolution reduces the propagation speed of internal Kelvin waves (Hsieh *et al* (1983), which are known to be important in the initial phase of the THC adjustment process (Kawase (1987); Döscher *et al* (1994); Johnson and Marshall (2001)). There is a possibility that details of the timing in the transient response are important by affecting the rate of weakening of the subtropical gyre. To determine to what extent this is the case requires experiments with improved resolution and physics schemes.

Detailed analyses of GCMs, such as in this experiment or in those described by Thorpe *et al* (2001) have emphasized the important role of processes that are not always included in simpler models, e.g. freshwater transport by the subtropical gyre.

Acknowledgements

We thank many of our colleagues at the Hadley Centre for their help with analysing this experiment. In particular we like to thank Robert Thorpe, Doug Cresswell, Anne Pardaens, John Mitchell and Chris Hewitt. Comments by Ron Stouffer and an anonymous reviewer have helped to improve the manuscript and are greatly appreciated. This work was funded by the Department for Environment, Food and Rural Affairs under the Climate Prediction Programme PECD/7/12/37.

References

Banks, H. T., 2000a: Indonesian Throughflow in a coupled climate model and the sensitivity of the heat budget and deep overturning. *J. Geoph. Res.*, **105**, 26,135–26,150.

——, 2000b: Ocean heat transport in the South Atlantic in a coupled climate model. *J. Geoph. Res.*, **105(C1)**, 1071–1091.

Bell, M. J., 1999: Vortex stretching and bottom pressure torques in the Bryan-Cox ocean circulation model. *J. Geophys. Res.*, **104**, 23,545–23,563.

Boyle, E., 2000: Is ocean thermohaline circulation linked to abrupt stadial/interstadial transitions? *Quaternary Sci. Rev.*, **19**, 255–272.

Broecker, W. S., 1991: The great ocean conveyor. *Oceanography*, **4**, 79–89.

Cortijo, E., L. Labeyrie, M. Elliot, E. Balbon, and N. Tisnerat, 2000: Rapid climatic variability of the North Atlantic Ocean and global climate: a focus of the IMAGES program. *Quaternary Sci. Rev.*, **19**, 227–241.

Cox, M. D., 1984: A primitive equation, three dimensional model of the ocean. Ocean Group Technical Report 1, 141pp, GFDL, Princeton.

Cubasch, U., G. A. Meehl, G. J. Boer, R. J. Stouffer, M. Dix, A. Noda, C. A. Senior, S. C. B. Raper, and K. S. Yap, 2001: Projections of future climate change. *Climate change 2001: The scientific basis. Contribution of Working Group I to the Third Assessment Report of the Intergovernmental Panel on Climate Change*, Houghton, J. T., Y. Ding, D. J. Griggs, M. Noguer, P. van der Linden, X. Dai, K. Maskell, and C. I. Johnson, Eds., Cambridge University Press. In press.

de las Heras, M. M., and R. Schlitzer, 1999: On the importance of intermediate water flows for the global ocean overturning. *J. Geoph. Res.*, **104**(C7), 15515–15536.

Dijkstra, H., and J. Neelin, 1999: Imperfections of the thermohaline circulation: multiple equilibria and flux correction. *J. Climate*, **12**, 1382–1392.

——, and ——, 2000: Imperfections of the thermohaline circulation: latitudinal asymmetry and preferred northern sinking. *J. Climate*, **13**, 366–382.

Döscher, R., C. W. Böning, and P. Herrman, 1994: Response of meridional overturning and heat transport in the North Atlantic to changes in thermohaline forcing in northern latitudes: A model study. *J. Phys. Oceanogr.*, **24**, 2306–2320.

Ganachaud, A., and C. Wunsch, 2000: Improved estimates of global ocean circulation, heat transport and mixing from hydrographic data. *Nature*, **408**, 453–457.

Ganapolski, A., and S. Rahmstorf, 2001: Rapid changes of glacial climate simulated in a coupled climate model. *Nature*, **409**, 153–158.

Gill, A. E., 1980: Some simple solutions for heat-induced tropical circulation. *Quart. J. Roy. Meteorol. Soc.*, **106**, 447–462.

Gordon, C., C. Cooper, C. A. Senior, H. Banks, J. M. Gregory, T. C. Johns, J. F. B. Mitchell, and R. A. Wood, 2000: The simulation of SST, sea ice extents and ocean heat transports in a version of the Hadley Centre coupled model without flux adjustments. *Clim. Dyn.*, **16**, 147–168.

Gregory, J. M., and J. F. B. Mitchell, 1997: The climate response to CO_2 of the Hadley Centre coupled AOGCM with and without flux adjustment. *Geophys Res Lett*, **24**, 1943–1946.

Hewitt, D., A. Broccoli, J. Mitchell, and R. Stouffer, 2001: A coupled model study of the last glacial maximum: was part of the North Atlantic relatively warm? *Geophys. Res. Lett*, **28**, 1571–1574.

Holland, W., 1973: Baroclinic and topographic influences on the transport in western boundary currents. *Geophys. Fluid Dyn.*, **4**, 187–210.

Hou, A., and R. S. Lindzen, 1992: The influence of concentrated heating on the Hadley circulation. *J. Atm. Sciences.*, **49**, 1233–1241.

Hsieh, W., M. Davey, and R. Wajsowicz, 1983: The free Kelvin wave in finite-difference numerical models. *J. Phys. Oceanogr.*, **13**, 1383–1397.

Hughes, T., and A. Weaver, 1994: Multiple equilibria of an asymmetric two-basin model. *J. Phys. Oceanogr.*, **24**, 619–637.

Johnson, H., and D. Marshall, 2001: A theory for the surface Atlantic response to thermohaline variability. *subm. J. Phys. Oceanogr.*

Kawase, M., 1987: Establishment of deep ocean circulation driven by deep-water production. *J. Phys. Oceanogr.*, **17**, 2294–2317.

Keigwin, L., G. Jones, and S. Lehman, 1991: Deglacial meltwater discharge, North Atlantic deep circulation and abrupt climate change. *J. Geophys. Res.*, **96**, 16811–16826.

Macdonald, A. M., 1998: The global ocean circulation: a hydrographic estimate and regional analysis. *Progress in Oceanography*, **41**, 281–382.

Manabe, S., and R. J. Stouffer, 1988: Two stable equilibria of a coupled ocean-atmosphere model. *J. Climate*, **1**, 841–866.

——, and ——, 1995: Simulation of abrupt climatic change induced by freshwater input to the North Atlantic Oocean. *Nature*, **378**, 165–167.

——, and R. Stouffer, 1997: Coupled ocean-atmosphere model response to freshwater input: comparison with Younger Dryas event. *Paleoceanography*, **12**, 321–336.

——, and R. J. Stouffer, 1999a: Are two modes of thermohaline circulation stable? *Tellus*, **51 A**, 400–411.

——, and ——, 1999b: The role of the thermohaline circulation in climate. *Tellus*, **51**, 91–109.

Muscheler, R., J. Beer, G. Wagner, and R. Finkel, 2000: Changes in deep-water formation during the Younger Dryas event inferred from ^{10}Be and ^{14}C records. *Nature*, **408**, 567–570.

Pardaens, A., H. Banks, J. Gregory, and P. Rowntree, 2001: Freshwater transports in HadCM3. *subm. Clim. Dyn.*

Pedlosky, J., 1987: *Geophysical fluid dynamics*. Springer-Verlag, New York.

Pope, V. D., M. L. Gallani, P. R. Rowntree, and R. A. Stratton, 2000: The impact of new physical parametrizations in the Hadley Centre climate model – HadAM3. *Climate Dyn.*, **16**, 123–146.

Rahmstorf, S., 1996: On the freshwater forcing and transport of the Atlantic thermohaline circulation. *Clim. Dyn.*, **12**, 799–811.

Schiller, A., U. Mikolajewicz, and R. Voss, 1997: The stability of the thermohaline circulation in a coupled ocean-atmosphere general circulation model. *Clim. Dyn.*, **13**, 325–347.

Schmittner, A., C. Appenzeller, and T. Stocker, 2000: Enhanced Atlantic freshwater export during El Niño. *Geophys. Res. Let.*, **27**(9), 1163–1166.

Thorpe, R. B., J. M. Gregory, T. C. Johns, R. A. Wood, and J. F. B. Mitchell, 2001: Mechanisms determining the Atlantic thermohaline circulation response to greenhouse gas forcing in a non-fluxadjusted coupled climate model. *acc. J. Climate*.

Vellinga, M., and R. Wood, 2001: Global climatic impacts of a collapse of the Atlantic thermohaline circulation. *subm. Climatic Change*.

Weijer, W., W. de Ruijter, H.Dijkstra, and P. van Leeuwen, 1999: Impact of interbasin exchange on the Atlantic overturning circulation. *J. Phys. Oceanogr.*, **29**, 2266–2284.

Wood, R. A., A. B. Keen, J. F. B. Mitchell, and J. M. Gregory, 1999: Changing spatial structure of the thermohaline circulation in response to atmospheric CO_2 forcing in a climate model. *Nature*, **399**, 572–575.

List of Figures

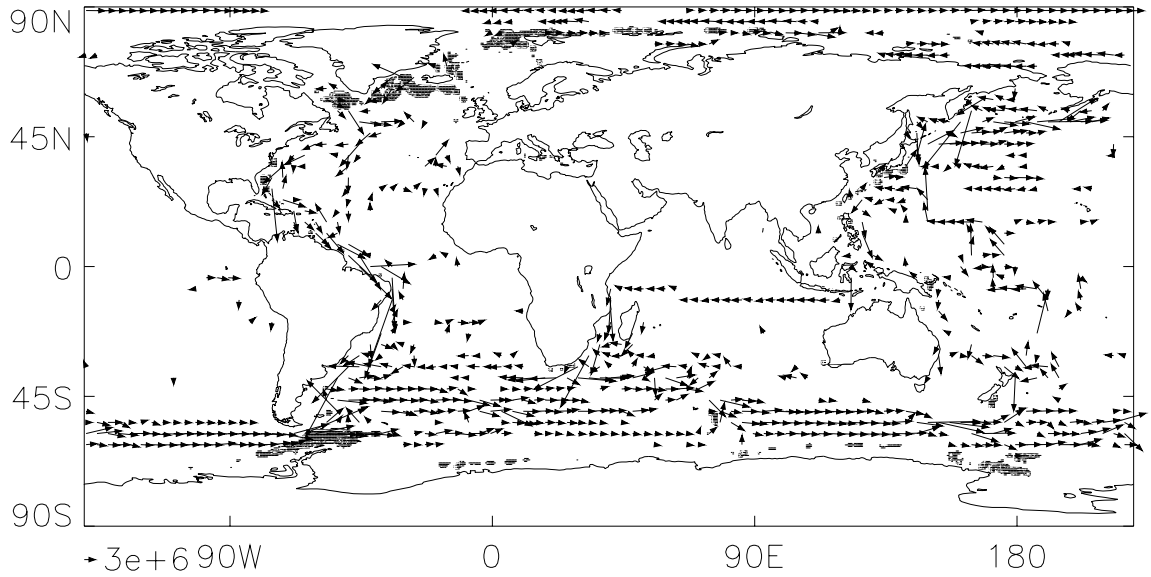

(a)

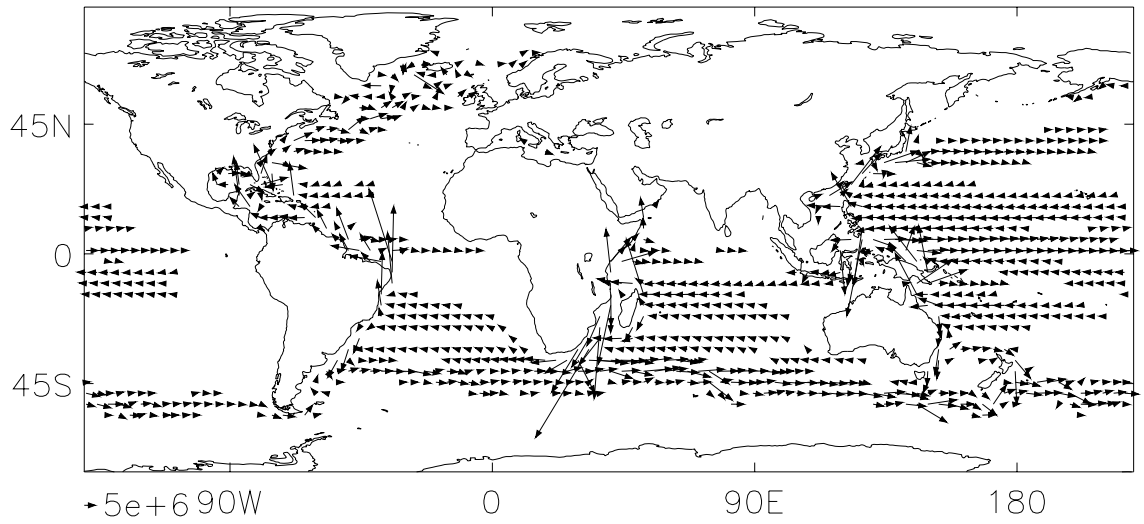

(b)

Figure 1: Horizontal mass transport across grid boxes in the control run (years 100-130), summed for two potential temperature (θ) categories: (a) $\theta < 5.5^oC$ (b) $\geq 5.5^oC$. Units are Sv. For clarity only every third arrow is shown and transports smaller than $1.5\,Sv$ are omitted. South of 40^oS the arrows of the cold flow (a) are scaled down by a factor of 5. The shaded areas in (a) indicate where convection warms the upper $1000\,m$ in excess of $1\,K/Gs$.

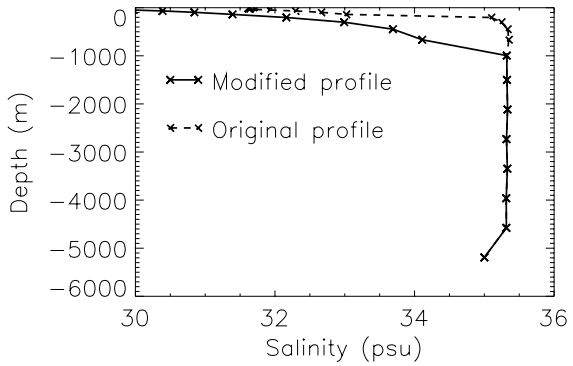

Figure 2: Area-averaged salinity profiles for the North Atlantic ($[80^oW - 20^oE] \times [55^oN - 90^oN]$). Dashed: original profile from the control run. Solid: modified profile, used to initialise the perturbation experiment.

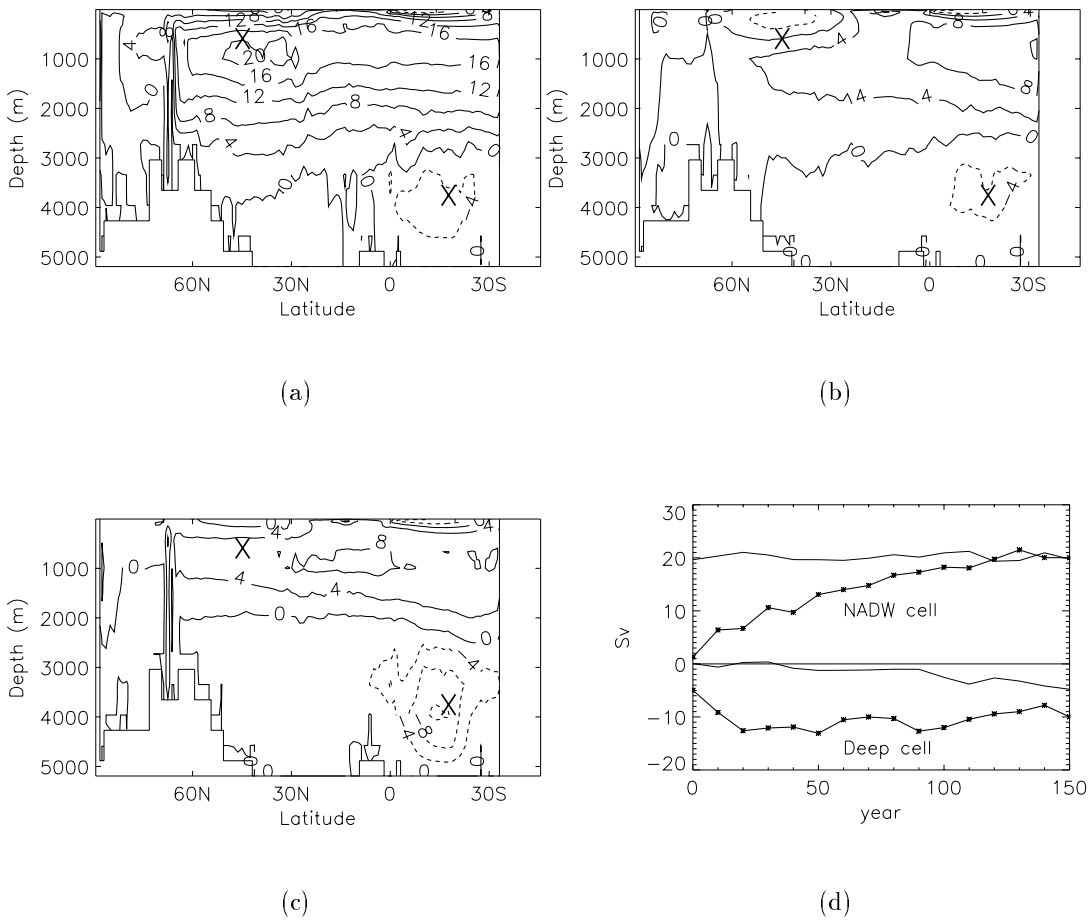

Figure 3: Meridional streamfunction in the Atlantic Ocean (positive value corresponds to counter-clockwise circulation). (a): averaged over 50 years of the control run. (b): Average over years 0-10 of the perturbation experiment. (c): Averaged over years 20-30 of the perturbation experiment. Positive (negative) values have solid (dashed) contours and indicate counter-clockwise (clockwise) circulation. Crosses indicate the points where (d) timeseries of the meridional streamfunction have been determined. The intensity of the NADW cell is shown by the positive curves; that of the deep cell by the negative curves. The bold curves with the asterisks are for the perturbation run, the thin curves for the control run.

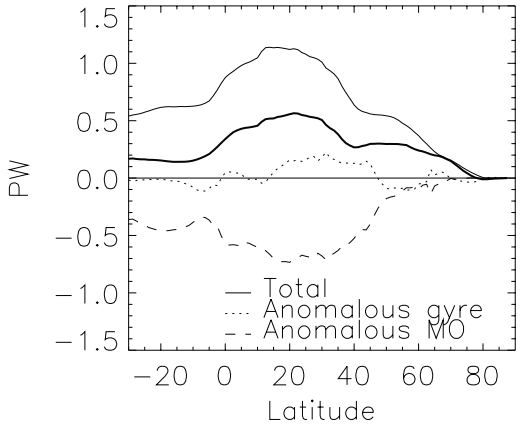

(a) Heat transport

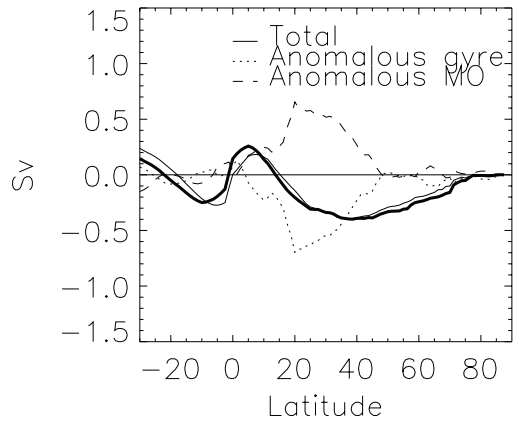

(b) Freshwater transport

Figure 4: (a) Ocean meridional heat transport in the Atlantic: average transport in year 20-30 of the perturbation run (solid, heavy), long-term average of the control run (solid, thin), change in the meridional overturning (dashed) and gyre (dotted) components of the perturbation run in year 20-30 (relative to their average values in the control run). (b) As a, but for the meridional freshwater transport.

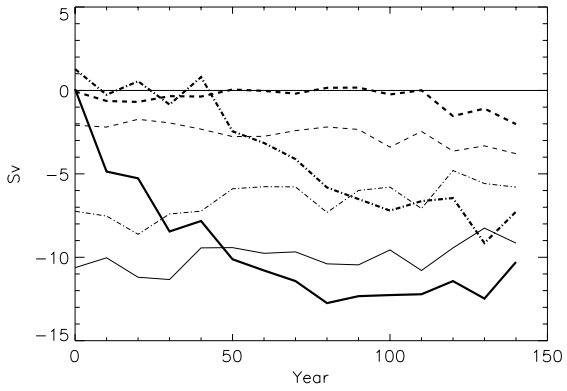

Figure 5: Time series of downward volume fluxes in the: Greenland-Norwegian Sea (solid): $[40^oW, 20^oE] \times [65^oN, 75^oN]$, Labrador Sea (dashed): $[80^oW, 45^oW] \times [48^oN, 75^oN]$ and Reykyanes Basin and overflow sills (dash-dotted): $[45^oW, 0^oW] \times [48^oN, 65^oN]$. Values for the perturbation (control) experiment are shown by the heavy (thin) curves. Downwelling rates are defined as the horizontally integrated average vertical velocity below $200\,m$ (to exclude Ekman pumping).

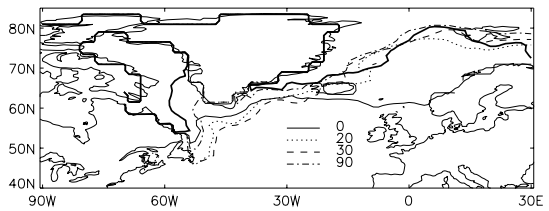

Figure 6: Contours of decadal mean DJF 25% sea ice cover for years 0-10, 20-30, 30-40, 90-100 of the perturbation run (see legend). The corresponding contour for the 100 year DJF mean of the control simulation is shown by the heavy solid line.

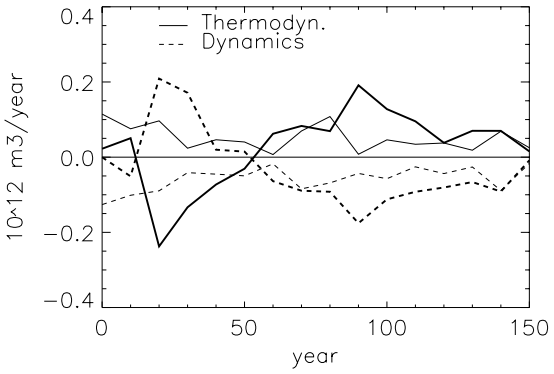

(a)

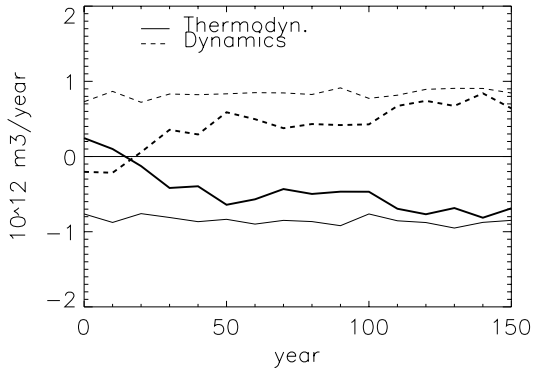

(b)

Figure 7: Sea ice growth rates in (a) the Labrador Sea and (b) GIN Sea due to transport 4(solid) and melting and freezing (dashed). Values for the perturbation (control) run are shown by the heavy (thin) lines.

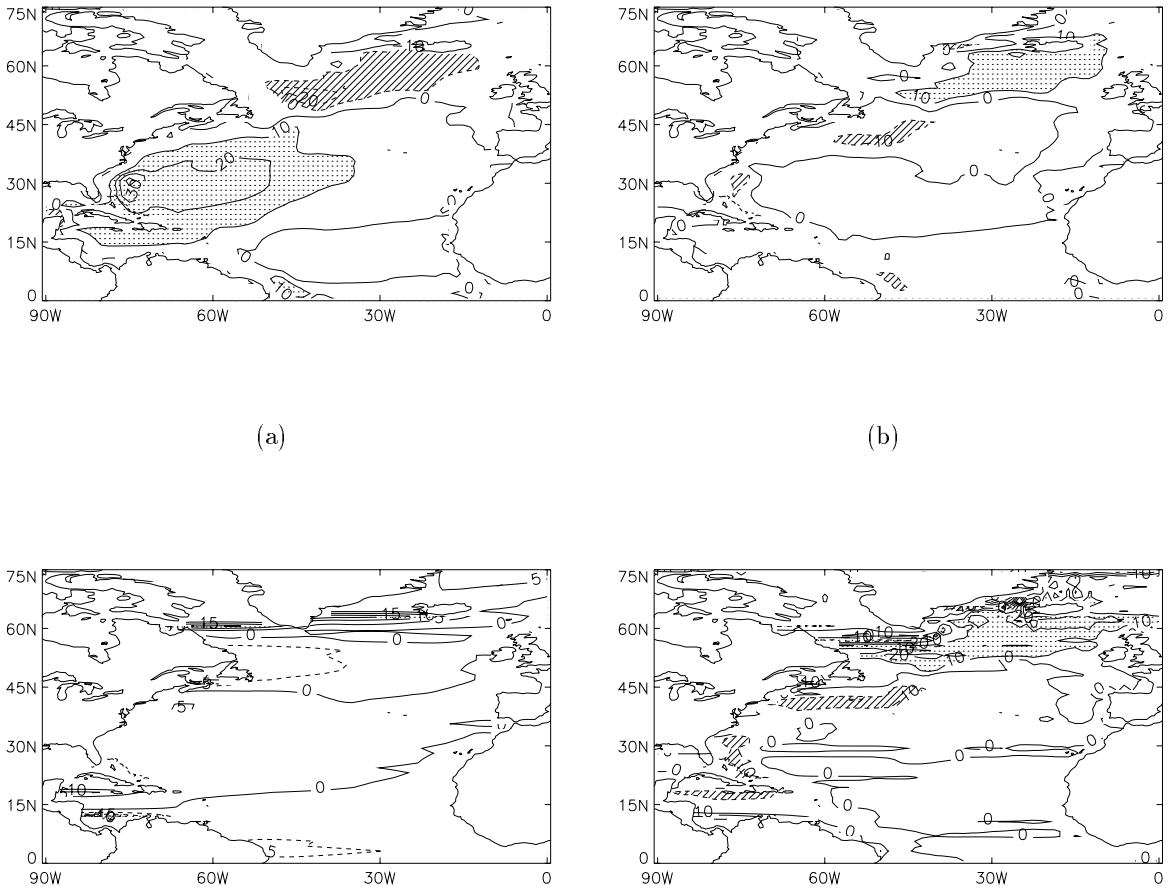

(a) (b)

(c) (d)

Figure 8: a: Barotropic streamfunction (in Sv) of the control run, parallel to years 1-10 of the perturbation run. b: Difference (perturbation minus control) during years 1-10. c: Anomalous barotropic circulation driven by wind stress curl ('Sverdrup flow') d: Anomalous circulation driven by bottom pressure torque. Contour interval is 10 Sv, except for c where it is 5 Sv.In stippled areas the streamfunction is larger than $10\,Sv$, in hatched areas it is smaller than $-10\,Sv$.

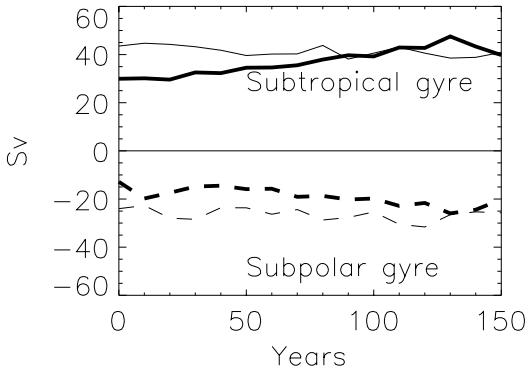

Figure 9: Extrema of the barotropic streamfunction in the North Atlantic, proxies for the strength of the subtropical (solid) and subpolar gyre (dashed). Values from the perturbation (control) run are shown by the heavy (light) curves.

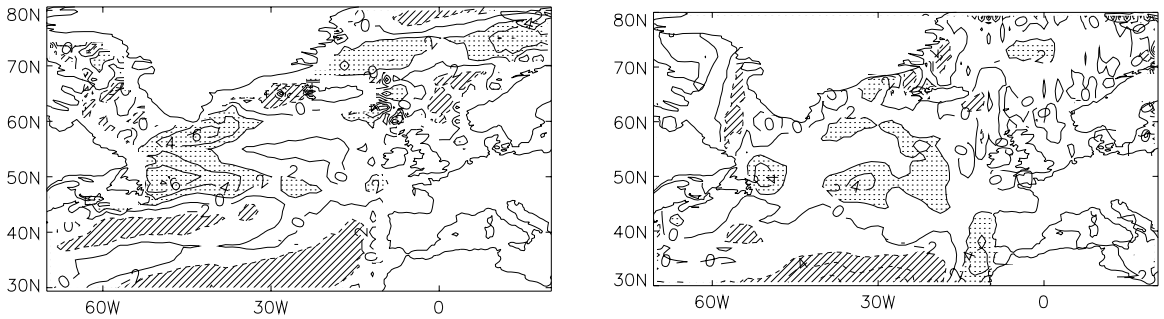

(a) (b)

Figure 10: Signal-to-noise ratios in years 20-30 (i.e. anomaly divided by standard deviation (SD) of control run) of (a) vertical Ekman velocity calculated from the wind stress (b) vertical velocity at $40m$. The field in (b) has been smoothed with a 5-point smoother to elminate grid-scale noise. Positive contours are solid, negative contours are dashed. In stippled areas the anomaly is positive and stronger than +2 SD, in the hatched areas negative and stronger than -2 SD.

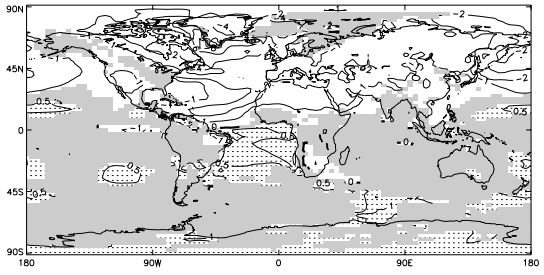

Figure 11: Change in surface air temperature for years 20-30 of the experiment, relative to the control climate. Cooling is indicated by heavy contours, intervals $[-8, -6, -4, -2, -1^oC]$. Warming is indicated by stippling and thin contours, at intervals $[0.5, 1, 2^oC]$. Changes that are not significantly different from zero (at 95%) have been masked by grey.

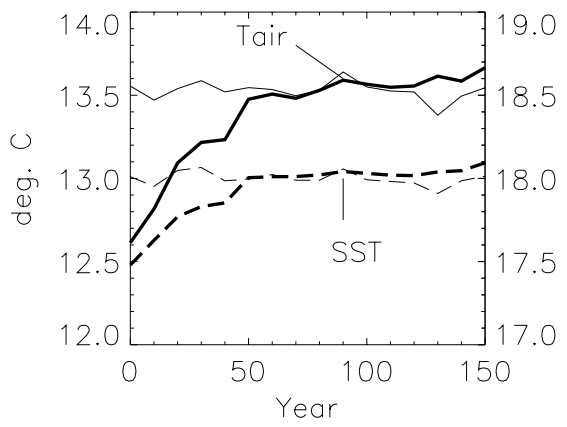

(a)

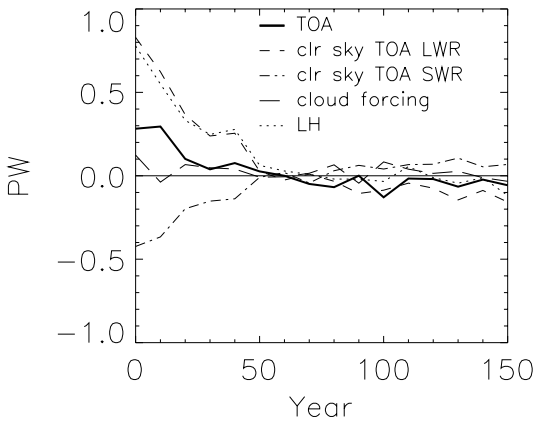

(b)

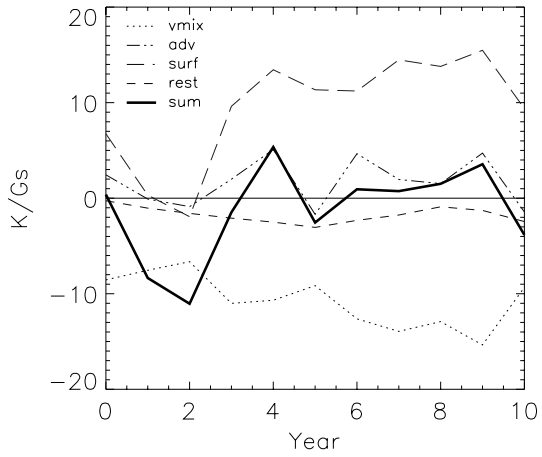

(c)

Figure 12: (a) Decadal mean global surface air temperature (solid, left-hand y-axis) and SST (dashed, right-hand y-axis). Thin: control run, thick: perturbation experiment. (b) Anomalies relative to the control (positive is downwards) of: net top-of-atmosphere ('TOA') flux (heavy solid), TOA clear-sky longwave radiative flux (dashed), TOA clear-sky short-wave radiation (dash-dot), TOA cloud radiative forcing (long dashes). Units in PW. The anomalous latent heat ('LH') flux into the ocean surface is shown by the dotted line. To take into account the smaller surface area of the ocean, integrated and not area averaged fluxes are shown. (c) Anomalies (perturbation minus average of control) of globally averaged heating rates (in K/Gs) in the top 35m of the ocean due to: vertical mixing (vmix), ie convection, mixed layer mixing and diffusion, vertical advection (adv), surface fluxes (surf), other terms (rest), and total rate of change (sum).

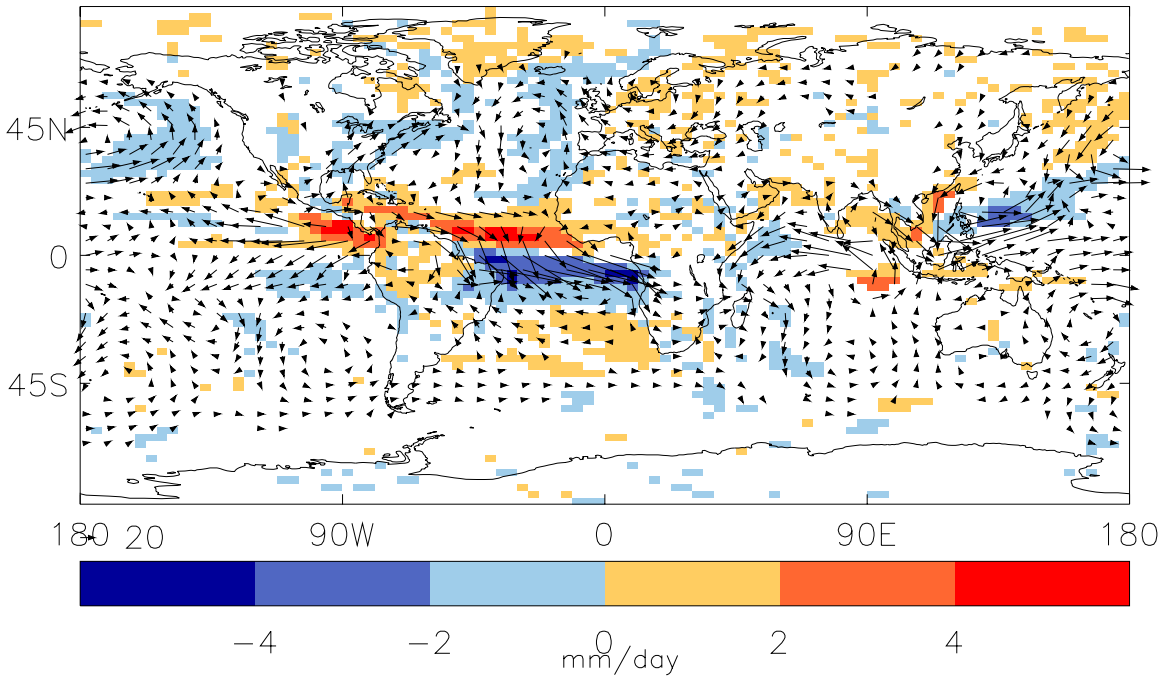

Figure 13: Vertically integrated anomalous atmospheric water vapour transport (arrows) during years 21-30 (perturbation minus control run). Colours represent the divergence of the anomalous water vapour transport (in mm/day), equal to $E - P$ anomalies at the surface if storage and horizontal transport of liquid water and snow are neglected. Only anomalies that are significantly different from the natural variability of the control climate are shown.

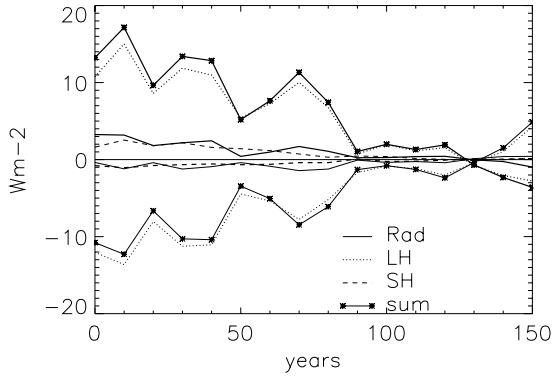

(a)

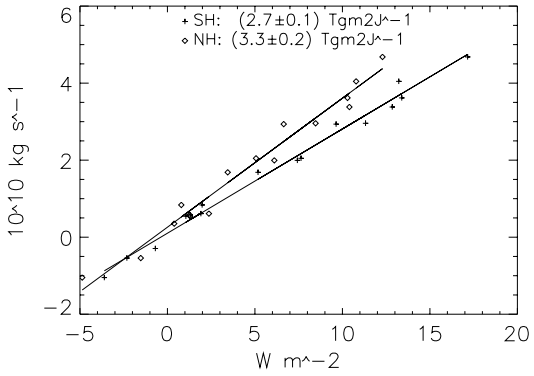

(b)

Figure 14: (a) Anomalies of vertically integrated zonal mean diabatic heating (solid, with asterisks), and the separate components: absorption of shortwave and longwave radiation (solid), release of latent heat ('LH', dotted) and of boundary layer heating ('SH', dashed). Values between the equator and 15^oN are shown by the thin curves (net anomalous cooling), between the equator and 15^oS by the thick curves (net anomalous heating). (b): Strength of anomalous Hadley cell vs. diabatic cooling anomalies north of the equator (diamonds) and heating south of the equator (crosses). The slope from a least-squares fit is shown at the top, with an estimate of the error.

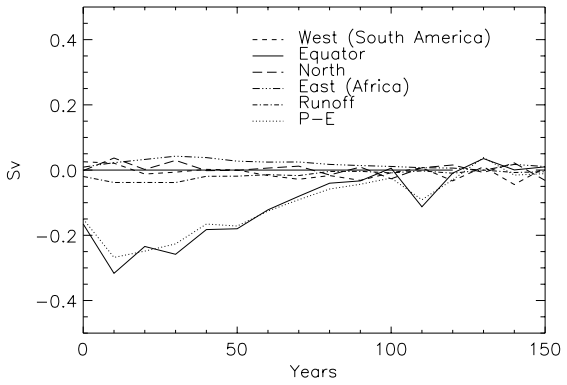

Figure 15: Anomalies (perturbation minus control mean) in the surface freshwater balance of the equatorial North Atlantic. This region is defined as the area between the equator, $20^o N$ and the coasts of Africa and South America. Shown (in Sv) are anomalies of total atmospheric water vapour transport across these sections *into* the area: the equator (solid), $20^o N$ (long dashes), the coasts of South America (short dashes) and of Africa (dash-dot-dot-dot); total river runoff (dash-dot). Also shown is the area-averaged net precipitation minus evaporation plus runoff anomaly experienced by the ocean (dotted).

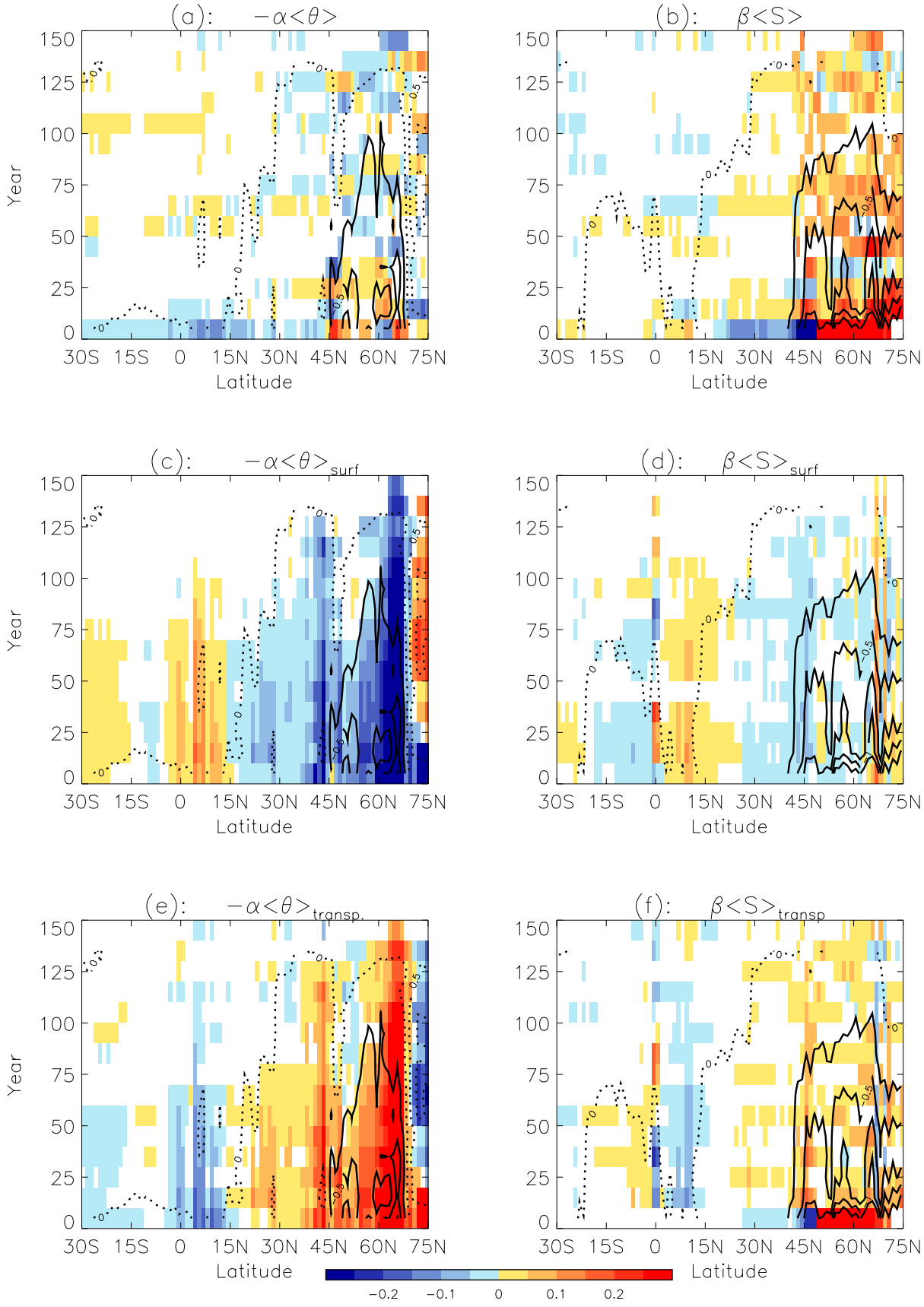

Figure 16: Hovmüller diagrams (colours) for the Atlantic Ocean showing anomalies with respect to the control run of the time derivatives of (a): $-\alpha\langle\bar{\theta}\rangle$. (b) $\beta\langle\bar{S}\rangle$. (c): $-\alpha\langle\bar{\theta}\rangle_{\rm surf}$. (d): $\beta\langle\bar{S}\rangle_{\rm surf}$(e): $-\alpha\langle\bar{\theta}\rangle_{\rm transp}$. (f): $\langle\bar{S}\rangle_{\rm transp}$. Units are $kg\,m^{-3}$decade^{-1}. Anomalies that are not significantly different from the natural variability of the control experiment have been masked. Values on colour bar are for (a) and (b), for (c)–(f) multiply values on bar with 2.5. Contours in (a),(c),(e) are anomalies of $\langle\bar{\theta}\rangle$ (interval 0.5^oC); contours in (b) (d) and (f) are anomalies of $\langle\bar{S}\rangle$ (interval 0.25 psu). Positive contours are dotted

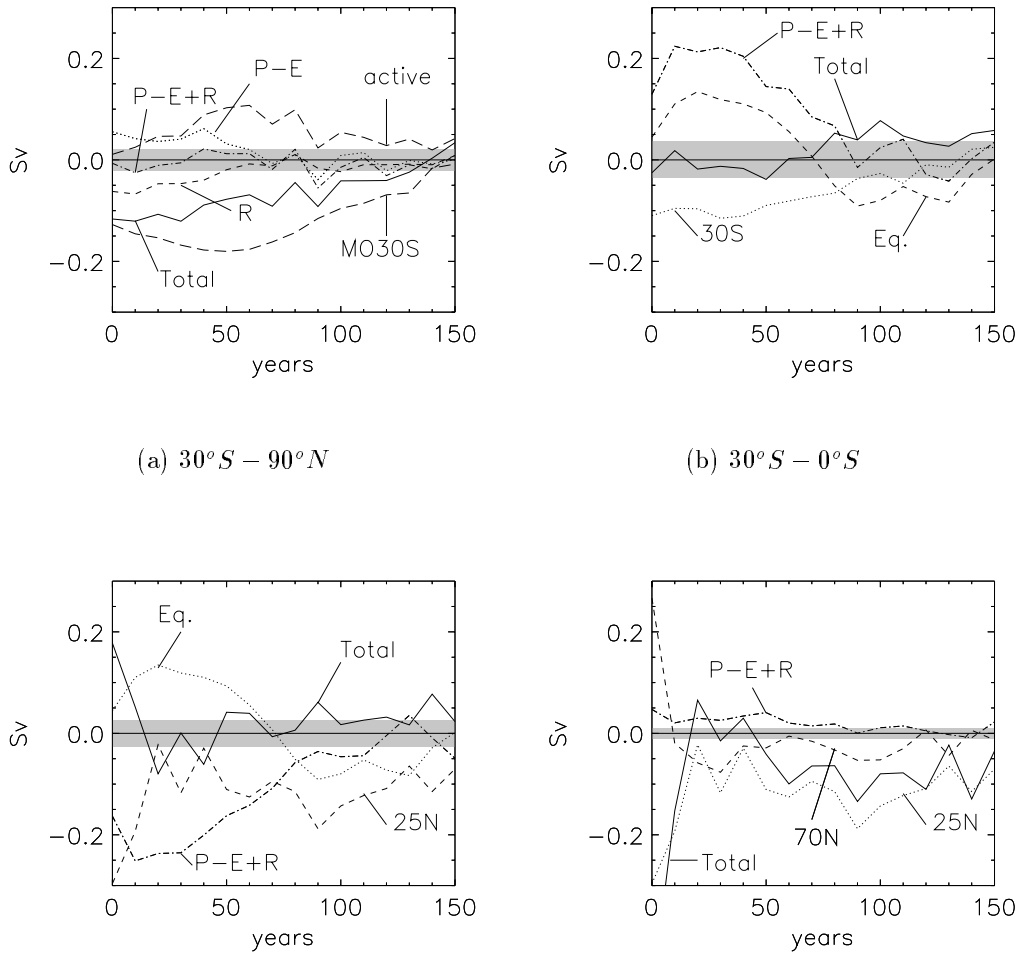

(a) $30^o S - 90^o N$

(b) $30^o S - 0^o S$

(c) $0^o N - 25^o N$

(d) $25^o N - 70^o N$

Figure 17: (a): Anomalies to the Atlantic freshwater budget between $30^o S - 90^o N$ including the Mediterranean and Arctic (perturbation minus average control values, in Sv): integrated $P - E$ (dotted), river runoff R (dashed), net surface flux $P - E + R$ (dash-dotted), and total freshwater input (integrated $P - E + R$ plus northward ocean freshwater transport across $30^o S$ (solid). Shading indicates the standard deviation of $P - E + R$ in the control run. Curve labelled 'MO30S' is the anomalous transport by the overturning at $30^o S$; 'active' is the anomalous input of freshwater into the Atlantic due to integrated $P - E + R$ and ocean freshwater transport at $30^o S$ other than by the meridional overturning.(b): As in (a) but for the South Atlantic, $30^o S - 0^o N$. Ocean freshwater transport across northern and southern boundaries of the area are shown by dotted and dashed lines. (c) As in b but for $0^o N - 25^o N$. (d) As in (c) but for $25^o N - 70^o N$.

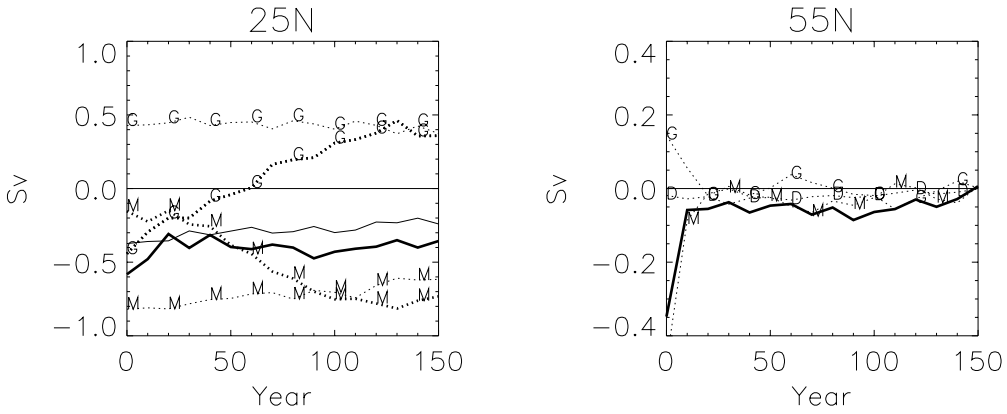

(a) $25^o N$ (b) $55^o N$

Figure 18: (a) Meridional freshwater transport in the Atlantic across $25^o N$. The total transport is shown by the solid lines, the separate components by the dotted curves labelled 'M' (meridional overturning), 'G' (gyre). Values from the perturbation (control) experiment are shown by heavy (thin) curves. (b) Anomalous transport across $55^o N$. 'D' is anomalous diffive transport.

List of Tables

Ocean section		$\theta \leq 3.5^oC$ Macdonald	$\theta \leq 5.5^oC$ Control	$\theta > 3.5^oC$ Macdonald	$\theta > 5.5^oC$ Control
Atlantic	48N	-27 (5)	-17.5 (2.1)	27 (5)	17.5(2.1)
	36N	-16 (4)	-16.2 (1.2)	15 (13)	16.2 (1.2)
	24N	-15 (7)	-14.8 (1.4)	15 (7)	14.8 (1.4)
	11N	-12 (12)	-17.3 (1.0)	10 (8)	17.3 (1.0)
	11S	-18 (14)	-17.7 (1.1)	17 (7)	17.7 (1.1)
	17S	-14 (10)	-17.4 (1.1)	13 (3)	17.4 (1.1)
	23S	-17 (14)	-16.5 (0.9)	16 (4)	16.5 (0.9)
Indian	32S	18 (14)	-0.4 (2.8)	-25 (11)	-23.3(2.8)
Pacific	43S	5 (12)	9.9 (1.4)	6 (11)	12.4 (1.4)
	28S	3 (23)	10.3 (1.4)	6 (11)	13.5 (1.4)
	10N	6 (43)	1.3 (2.9)	-6 (16)	-1.3 (2.9)
	24N	2 (27)	0.4 (1.6)	-1 (10)	-0.4 (1.6)
	47N	-4 (31)	-8.2 (1.0)	5 (4)	8.2 (1.0)
SO	68W	114 (11)	200 (5)	28 (6)	6.6 (3.8)
	30E	131 (116)	200 (3)	11 (20)	6.9 (1.6)
	132E	109 (92)	200 (4)	41 (34)	31 (2)

Table 1: Mass transport across selected ocean sections, partitioned into 'cold' and 'warm' classes. The table shows data presented by Macdonald (1998) and mean transports in years 100-130 of the control run of HadCM3 parallel. An estimate of the error is given in brackets. The error in the data from Macdonald (1998) is estimated from the errors of the separate currents across each section. For the HadCM3 control data we have taken the standard deviation over the 10 years. Units are $10^9 kg/sec$; northward and eastward transports are positive. 'SO' stands for Southern Ocean.